Advances in Applied Mathematics and Mechanics
Adv. Appl. Math. Mech., Vol. 7, No. 5, pp. 644-662

DOI: 10.4208/aamm.2014.m632
October 2015

Thermo-Solutal Natural Convection in an Anisotropic Porous Enclosure Due to Non-Uniform Temperature and Concentration at Bottom Wall

Ashok Kumar*, Pravez Alam and Prachi Fartyal

Department of Mathematics, HNB Garhwal University (A Central University), Srinagar–246174, Uttarakhand India

Received 26 May 2014; Accepted (in revised version) 3 November 2014

Abstract. This article summaries a numerical study of thermo-solutal natural convection in a square cavity filled with anisotropic porous medium. The side walls of the cavity are maintained at constant temperatures and concentrations, whereas bottom wall is a function of non-uniform (sinusoidal) temperature and concentration. The non-Darcy Brinkmann model is considered. The governing equations are solved numerically by spectral element method using the vorticity-stream-function approach. The controlling parameters for present study are Darcy number (Da), heat source intensity i.e., thermal Rayleigh number (Ra), permeability ratio (K^*), orientation angle (ϕ). The main attention is given to understand the impact of anisotropy parameters on average rates of heat transfer (bottom, Nu_b, side Nu_s) and mass transfer (bottom, Sh_b, side, Sh_s) as well as on streamlines, isotherms and iso-concentration. Numerical results show that, for irrespective value of K^*, the heat and mass transfer rates are negligible for $10^{-7} \leq Da \leq 10^{-5}$, $Ra = 2\times10^5$ and $\phi = 45^\circ$. However a significant impact appears on Nusselt and Sherwood numbers when Da lies between 10^{-5} to 10^{-4}. The maximum bottom heat and mass transfer rates (Nu_b, Su_b) is attained at $\phi = 45^\circ$, when $K^* = 0.5$ and 2.0. Furthermore, both heat and mass transfer rates increase on increasing Rayleigh number (Ra) for all the values of K^*. Overall, It is concluded from the above study that due to anisotropic permeability the flow dynamics becomes complex.

AMS subject classifications: 65M10, 78A48

Key words: Spectral element method, anisotropic porous medium, non-Darcy Brinkmann model, non-uniform heating.

1 Introduction

In many natural and technological processes, temperature and mass or concentration diffusion act together to induce a buoyancy force which drives the fluid, and it is known

*Corresponding author.
Email: ashrsdma@gmail.com (A. Kumar)

as double-diffusive or thermo-solutal convection. The basic feature of double-diffusive convection is that two components with different rates of diffusion affect the fluid density. In oceanography [1], convection processes involve thermal and salinity gradients. Double-diffusive convection is more complex than the single diffusive convective flow. From practical and industrial point of view, natural convection due to combined buoyancy effect of thermal and species diffusion in a fluid saturated porous medium is received considerable attention. The migration of moisture in fibrous insulation, contaminants transport in the environment, solidification of binary alloy and crystal growth, melting and cooling near ice surfaces, sea water intrusion into freshwater lakes, dispersion of dissolvent materials or particulate matter in flows etc. are few examples, where double-diffusive convection is involved. The recent comprehensive literature review on thermo-solutal convection in porous media has been conducted by Nield and Bejan [2].

In the above type of configuration generally two situations buoyancy assisted and buoyancy opposed are considered. Several experimental and numerically studies in this field (without porous medium) are reported by Kamotani et al. [3], Lee et al. [4], Beghein et al. [5], Bennacer and Gobin (see [6, 7]), and Ghorayeb and Mojtabi [8] etc. Double-diffusive natural convection in a cubic enclosure subject to opposing and horizontal gradients of heat and solut is studied by Sezai and Mohamad [9]. Natural convection with combine heat and mass transfer in a vertical slot filled with isotropic porous medium, whose vertical walls are subjected to uniform fluxes of heat and mass, while the horizontal walls are insulated and impermeable, is analyzed by Trevisan and Bejan [10], Mehta and Nandkishor [11] and Mamou et al. (see [12, 13]) etc.

A comprehensive studies on thermo-solutal natural convection in a rectangular cavity filled with isotropic porous medium where different but uniform temperature and concentration are specified at two vertical walls and horizontal walls are adiabatic, are analyzed by Trevisan and Bejan [14], Goyeau et al. [15], and Kramer et al. [16]. Alavyoon [17] has reported the existence of analytical solution for slender cavity, when flow is induced by heat and mass fluxes on the vertical walls. Later on, for opposing heat and mass fluxes on the vertical walls, flow oscillation was reported by Alavyoon et al. [18].

Similar type of problems have also been investigated to understand anisotropic behavior of the medium in double-diffusive natural convection by Nitiarasu et al. [19], Bera et al. [20–22]) and Bennacer et al. [23] etc. Nithiarasu et al. [19] have studied the double-diffusive natural convective flow within a rectangular enclosure using a non-Darcy generalized model. They have reported that non-Darcy effects on flow, heat and mass transfer are significant, when the Rayleigh or Darcy numbers are large. Bera et al. [20] have presented significant effect of orientation angle as well as anisotropic permeability on flow rate, and on the overall heat and mass transfer rates. A numerical and analytical investigation on double diffusive natural convection, induced by buoyancy forces along with hydrodynamic, thermal, and solute anisotropy, is examined by Bera et al. [21]. They have shown the significant effect of anisotropic orientation angles of thermal and solute diffusivity on the overall heat and mass transfer rates. Later on, this investigation is extended by Bera and Khalili [22] and reported that, the existence of multiple steady so-

lutions as well as oscillating unsteady solution in certain range of controlling parameters. Bennacer et al. [23] have analyzed the effect of anisotropy on heat and mass transfer rates. Their numerical results indicate the existence of three regimes, namely, diffusive one for low value of permeability ratio, a transition regime when Sh and Nu (Sherwood and Nusselt numbers) increase as increasing the permeability, and asymptotic regime when Sh and Nu become independent of permeability ratio. Mojtaba et al. [25] have examined a thermo solutal convection in rectangular cavity. They have shown, that the anisotropic properties of the porous medium considerably modify the heat and mass transfer rates from that expected under isotropic conditions. Recently, a double diffusive convection in anisotropic porous rectangular cavity is examined by Safi et al. [26]. They have found that the heat and mass transfer are weak functions of the Darcy number for high and low conductivity regimes.

The present study reveals the physics of the thermo-solutal natural convective flow within a porous enclosure due to equal and non-uniform (sinusoidal) temperature and concentration at bottom wall along with uniform temperature and concentration at side walls. It is an extension of our previous work [24], by incorporating the mass transfer into the system. The Non-Darcy Brinkmann extended model has been adopted to simulate the momentum transfer in the porous medium. The Spectral element method (see [27,28]) is used to solve the governing equations.

2 Mathematical formulation

We consider a steady state natural convective flow in a square cavity of length L, filled with porous medium as shown schematically in Fig. 1. The flow is induced by constant temperatures and concentrations at side walls along with the non-uniform (sinusoidal) temperature and concentration at the bottom wall of the cavity. The non-Darcy

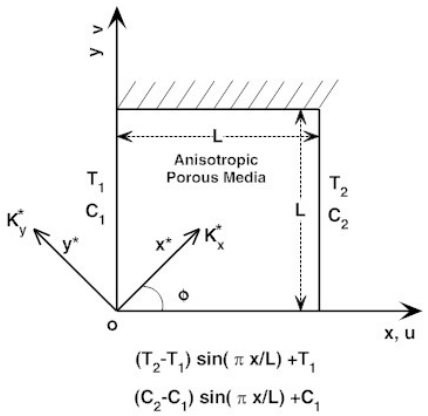

Figure 1: Physical model and co-ordinate system.

Brinkmann model is considered. The medium is anisotropic in permeability, which is due to the consequence of a preferential orientation or asymmetric geometry of the grain in geothermal system. The second order permeability tensor, $\overline{\overline{K}}$, is diagonal in the (ox^*,oy^*) coordinate system, with the diagonal components, K_{x^*} and K_{y^*}, respectively. Since the media is anisotropic, diffusion property is also expected to be anisotropic in nature (see [29,30]). However, our main emphasis is given on the impact of anisotropic media permeability on the heat and mass transfer rates and fluid flow. In order to reduce the number of influencing parameters, isotropic thermal and mass diffusivities are considered.

The fluid and porous medium are everywhere in local thermodynamic equilibrium, i.e., the temperature of the fluid and the porous medium at the interface are locally equal. The thermo-physical properties of the fluid are assumed to be constant except for the density dependence of the buoyancy body-force term in the momentum equation, which is satisfied by the Boussinesq approximation. The governing equations for the steady-state flow, heat and mass transfers are given by

$$\nabla\cdot\mathbf{V}=0, \tag{2.1a}$$

$$(\mathbf{V}\cdot\nabla)\mathbf{V}=-\frac{1}{\rho}\nabla p+\nu\nabla^2\mathbf{V}-\frac{\nu}{\overline{\overline{K}}}\mathbf{V}-\rho g\mathbf{Q}, \tag{2.1b}$$

$$\mathbf{V}\cdot\nabla T=\alpha\nabla^2 T, \tag{2.1c}$$

$$\mathbf{V}\cdot\nabla C=D\nabla^2 C, \tag{2.1d}$$

$$\rho=\rho_0[1-\beta_T(T-T_1)-\beta_C(C-C_1)], \tag{2.1e}$$

with the boundary conditions

$$u(0,y)=u(L,y)=u(x,0)=u(x,L)=0, \qquad v(0,y)=v(L,y)=v(x,0)=v(x,L)=0,$$

$$T(x,0)=(T_2-T_1)\sin\left(\frac{\pi x}{L}\right)+T_1, \qquad C(x,0)=(C_2-C_1)\sin\left(\frac{\pi x}{L}\right)+C_1,$$

$$T(0,y)=T(L,y)=T_1, \qquad C(0,y)=C(L,y)=C_1,$$

$$\frac{\partial T}{\partial x}=0 \quad \text{at } y=L, \qquad \frac{\partial C}{\partial x}=0 \quad \text{at } y=L.$$

In the above equations, $\mathbf{V}(\mathbf{u},\mathbf{v})$, p, T, C, α, D, $\mathbf{Q}$ and ρ are the flow velocity, pressure, temperature, concentration, thermal diffusivity, solutal diffusivity, unit vector along gravity and fluid density respectively. The permeability tensor, $\overline{\overline{K}}$, is defined as

$$\overline{\overline{K}}=K_{x^*}\begin{bmatrix} a & c \\ c & b \end{bmatrix}$$

with

$$a=K^*\sin^2\phi+\cos^2\phi, \quad b=K^*\cos^2\phi+\sin^2\phi, \quad c=(1-K^*)\sin\phi\cos\phi,$$

where ϕ is orientation angle. Using non-dimensional quantities

$$X=\frac{x}{L}, \qquad Y=\frac{y}{L}, \qquad U=\frac{Lu}{\alpha}, \qquad V=\frac{Lv}{\alpha},$$
$$P=\frac{pL^2}{\rho\alpha^2}, \qquad \theta=\frac{T-T_1}{T_2-T_1}, \qquad c=\frac{C-C_1}{C_2-C_1}, \qquad N=\frac{\beta_C(C_2-C_1)}{\beta_T(T_2-T_1)},$$
$$Ra=\rho_0\beta_T L^3\frac{(T_2-T_1)}{\alpha\nu}, \qquad Da=\frac{K_{y^*}}{L^2}, \qquad Le=\frac{\alpha}{D}, \qquad Pr=\frac{\nu}{\alpha},$$

the above differential equations can be written as:

$$\frac{\partial U}{\partial X}+\frac{\partial V}{\partial Y}=0, \tag{2.2a}$$
$$U\frac{\partial U}{\partial X}+V\frac{\partial U}{\partial Y}=-\frac{\partial P}{\partial X}+Pr[\nabla^2 U]-\frac{Pr}{Da}(bU-cV), \tag{2.2b}$$
$$U\frac{\partial V}{\partial X}+V\frac{\partial V}{\partial Y}=-\frac{\partial P}{\partial Y}+Pr[\nabla^2 V]-\frac{Pr}{Da}(-cU+aV)+RaPr(\theta+NC), \tag{2.2c}$$
$$U\frac{\partial \theta}{\partial X}+V\frac{\partial \theta}{\partial Y}=\frac{\partial^2\theta}{\partial^2 X}+\frac{\partial^2\theta}{\partial^2 Y}, \tag{2.2d}$$
$$U\frac{\partial c}{\partial X}+V\frac{\partial c}{\partial Y}=\frac{1}{Le}\Big(\frac{\partial^2 c}{\partial^2 X}+\frac{\partial^2 c}{\partial^2 Y}\Big), \tag{2.2e}$$

in which Ra, Da, K^*, Pr, N, Le are Rayleigh number, Darcy number, permeability ratio, Prandtl number, buoyancy ratio number respectively.

The momentum equations (2.2b), (2.2c) may be rewritten in terms of dimensionless vorticity, (ω) and stream function, ψ, as

$$U\frac{\partial \omega}{\partial X}+V\frac{\partial \omega}{\partial Y}=Pr[\nabla^2\omega]+\frac{Pr}{Da}\Big[b\frac{\partial^2\psi}{\partial^2 Y}+2c\frac{\partial^2\psi}{\partial X\partial Y}+a\frac{\partial^2\psi}{\partial^2 X}\Big]-RaPr\Big(\frac{\partial\theta}{\partial X}+N\frac{\partial C}{\partial X}\Big), \tag{2.3a}$$
$$\omega\equiv\frac{\partial U}{\partial Y}-\frac{\partial V}{\partial X}=-\frac{\partial^2\psi}{\partial Y^2}-\frac{\partial^2\psi}{\partial X^2}. \tag{2.3b}$$

We can obtain ψ from ω by solving the Poisson equation

$$\nabla^2\psi=-\omega. \tag{2.4}$$

The non-dimensional boundary conditions over the walls of enclosure are

$$\psi=0,\ \ \theta=0,\ \ C=0 \ \text{ and } \ \omega=-\frac{\partial^2\psi}{\partial X^2} \ \text{ at } \ X=0,$$
$$\psi=0,\ \ \theta=0,\ \ C=0 \ \text{ and } \ \omega=-\frac{\partial^2\psi}{\partial X^2} \ \text{ at } \ X=1,$$
$$\psi=0,\ \ \theta=\sin(\pi X),\ \ C=\sin(\pi X) \ \text{ and } \ \omega=-\frac{\partial^2\psi}{\partial Y^2} \ \text{ at } \ Y=0,$$
$$\psi=0 \ \ \frac{\partial\theta}{\partial Y}=0,\ \ \frac{\partial C}{\partial Y}=0 \ \text{ and } \ \omega=-\frac{\partial^2\psi}{\partial Y^2} \ \text{ at } \ Y=1.$$

The average bottom as well as side Nusselt numbers, (Nu_b, Nu_s) and Sherwood numbers, (Sh_b, Sh_s) are defined as follows:

$$Nu_b = \int_0^1 \left[-\frac{\partial\theta}{\partial Y}\right]_{Y=0} dX, \qquad Nu_s = \int_0^1 \left[-\frac{\partial\theta}{\partial X}\right]_{X=0} dY, \tag{2.5a}$$

$$Sh_b = \int_0^1 \left[-\frac{\partial C}{\partial Y}\right]_{Y=0} dX, \qquad Sh_s = \int_0^1 \left[-\frac{\partial C}{\partial X}\right]_{X=0} dY. \tag{2.5b}$$

We compute the above integrals by using Chebyshev-Gauss-Lobatto integration.

2.1 Numerical solution

The governing partial differential equations (2.2d)-(2.4), along with hydrodynamic and thermal boundary conditions are solved by the spectral element method (see [27]). The spectral element method is a synthesis of the spectral and the finite element methods. It is also called the p-type finite element method, or the h-p type weighted residual method. The name p-type means that accuracy is increased by increasing the order of the approximating polynomials (thus, p) rather than decreasing the mesh size, h. The spectral element method is a high order finite element technique that combines the geometric flexibility of finite elements with the high accuracy of spectral methods. This method was pioneered by A. T. Patera (see [27]). It is an elegant formulation of the finite element method with a high order piecewise polynomial basis. The hybrid character of the SEM enables it to overcome the disadvantages of both the spectral method and finite element method but still retain their advantages. Since the trial functions in SEM are local it can handle complex geometry easily. In this method the domain is decomposed into finite numbers of elements (also called sub-domains) and the spectral approximation is applied on each of sub-domains, and within each sub-domains the dependent variable is represented as a high-order Lagrangian interpolate in terms of Chebyshev polynomials, the coefficients of which are related to the function values at the Gauss-Lobatto Chebyshev collocation points. Spectral accuracy can be achieved when the solution possesses no singularities. Therefore, for those sub-domains where the solutions are not smooth, the high order accuracy of spectral methods will be destroyed. The main difference between SEM and spectral multi-domain method is that the C^0 and C^1 boundary conditions at the interfaces of the elements have to be explicitly enforced by the spectral multi-domain method. The spectral element method, by contrast, use the variational principle to guarantee C^0 and C^1 (weakly) continuity at the interface. To solve the above governing equations (2.2d)-(2.4), using spectral element method, a pseudo-transient term ($\partial\zeta/\partial t$) of the corresponding field variable, is added in each equation. Then these pseudo-transient Cauchy-Kowalewski form of vorticity, stream and energy equations are discretized by a semi-implicit discretization in which a first-order finite-difference approximation, with time-step Δt, is used for the time derivative, the Laplacian term is treated implicitly (using unknown values at time step $n+1$) and all other terms treated explicitly (using known values at time step n). The time discretized form of the resulting equations is given by a

Helmholtz equation of the form:

$$\nabla^2\zeta^{(n+1)}-\lambda_\zeta^2\zeta^{(n+1)}=f_\zeta^{(n)}, \tag{2.6}$$

where ζ may represent any one of the fundamental field variables (ω, ψ, θ). Both terms on the left side of Eq. (2.6) contain unknown values of ζ at the new time-step $(n+1)$, while the forcing function f_ζ on the right hand side is evaluated using previous values. The vorticity equation (2.3a) is also made pseudo-transient, but some manipulation as to be used to overcome the complication due to anisotropic permeability. The Helmoltz equation corresponding to Eq. (2.3a) is follows:

$$\nabla^2\omega^{(n+1)}-\lambda_\omega^2\omega^{(n+1)}=f_\omega^{(n)}. \tag{2.7}$$

For the case (i) $b\geq a$:

$$\lambda_\omega^2=\Big(\frac{1}{\Delta t}-\frac{b}{Da}\Big),$$
$$f_\omega^{(n)}=-\Big[\frac{\omega}{\Delta t}+\frac{1}{Da}\Big((b-a)\frac{\partial^2\psi}{\partial Y^2}+2c\frac{\partial^2\psi}{\partial X\partial Y}\Big)+\frac{1}{Pr}\Big(U\frac{\partial\omega}{\partial X}+V\frac{\partial\omega}{\partial Y}\Big)-Ra\Big(\frac{\partial\theta}{\partial Y}+N\frac{\partial C}{\partial Y}\Big)\Big]^{(n)}.$$

For the case (ii) $b\leq a$:

$$\lambda_\omega^2=\Big(\frac{1}{\Delta t}-\frac{a}{Da}\Big),$$
$$f_\omega^{(n)}=-\Big[\frac{\omega}{\Delta t}+\frac{1}{Da}\Big((a-b)\frac{\partial^2\psi}{\partial Y^2}+2c\frac{\partial^2\psi}{\partial X\partial Y}\Big)+\frac{1}{Pr}\Big(U\frac{\partial\omega}{\partial X}+V\frac{\partial\omega}{\partial Y}\Big)-Ra\Big(\frac{\partial\theta}{\partial Y}+N\frac{\partial C}{\partial Y}\Big)\Big]^{(n)}.$$

For each equation, the corresponding Helmoltz equation is solved by spectral element method. The basic steps involved in SEM and solution procedure is given below:

Basic Steps:

1. Using time discretization obtain the corresponding Helmholtz equation of the PDE.
2. Obtain its equivalent functional in the main domain.
3. Split the domain into finite number of elements and obtain functional at each element.
4. Approximate the unknown function by eigen functions of some singular Strum-Liouville problem.
5. Approximate the derivative of unknown function by same way.
6. Obtain the elemental equations in each element by minimizing the functional.
7. Use boundary conditions.
8. Obtain the global matrix equations of the form of $AX=b$.
9. Solve the system by LU decomposition.

Solution Procedure:

Step 1 Specify the initial guess for the temperature, vorticity, stream-function, and velocities, $n=0$.

Step 2 Solve the energy equation for $n+1$th time-step.

Step 3 Solve the concentration equation for $(n+1)$-th time-step.

Step 4 Solve the vorticity equation for $(n+1)$-th time step.

Step 5 Solve the stream-function for $(n+1)$-th time step.

Step 6 Compute the velocity field and velocity gradient in the solution domain and vorticities at the boundaries.

Step 7 Check the convergence by the criterion,

$$\Delta_{rms}=\sqrt{\frac{\sum_{i=1}^{N_{\text{Total}}}[\zeta_i^{n+1}-\zeta_i^n]^2}{N_{\text{Total}}}}<\epsilon\Delta\tau, \tag{2.8}$$

update the variables i.e., $\zeta^n \leftarrow \zeta^{n+1}$ for all variables.

The Steps 2-6 are repeated until this convergence condition is satisfied by all variables, ζ. The details of this technique and its implication can be found elsewhere [20].

2.2 Validation of numerical solution

In this present paper, we have extended our recent work [24], by introducing the mass transfer in the system. In our recent work [24], a comprehensive numerical investigation on natural convection in a hydrodynamic anisotropic porous enclosure is presented. The same code of spectral element method is used to solve numerically the governing momentum and energy equations. The same code has been extend for solving the present problem in which only mass transfer equation is in addition. The validation of our code was shown in two ways. First, the independency of solution on grid size by changing order of polynomials. For the grid in-dependency we have taken different order of polynomial ranging from 7 to 12 in spectral approximation. Second, results of our special case are compared with the published one. The independency of the solution of this present problem on grid size by changing order of polynomial is same as in [24]. For the comparison with the published result of [20] we have translate our physical problem by changing boundary conditions (taking adiabatic bottom wall instead of non-uniform boundary condition) and the model suitably. As can be seen from Table 1, the agreement is very good. These tests give a strong validation of our numerical results.

Table 1: Comparison between present and published results of Bera et al. [20] at $Ra=10^5$, $Da=10^{-3}$, $Le=3$, $N=3$, and $\theta=60^\circ$.

K^*	Bera et al. [20] (Darcy-Brinkman-extended model) (Nu,Sh)	Present (Nu,Sh)
0.1	(3.78, 9.08)	(3.778, 9.076)
0.5	(3.88, 9.28)	(3.881, 9.277)
1.0	(4.00, 9.58)	(4.003, 9.576)
10	(1.70, 3.97)	(1,713, 3.968)

3 Results and discussion

A rigorous numerical studies is carried out to investigate the steady state behavior of the system, which is considered here. The heat and mass transfer, and fluid flow mechanisms are governed by Rayleigh number (Ra), aspect ratio (A), Prandtl number (Pr) and Darcy number (Da), permeability ratio (K^*) and orientation angle (ϕ). The main emphasize is given on the effect of media anisotropy and Rayleigh number (Ra) in terms of overall heat and mass transfer rates as well as on streamlines, isotherms and iso-concentration contours. The media anisotropy is governed by basically two parameters (i) K^* (ii) ϕ. In the entire result section, Prandtl number (Pr), Lewis number (Le) and buoyancy ratio (N) are fixed at 0.71, 2.0 and 2.0, respectively.

3.1 Effect of media permeability

The effect of media permeability is considered by studying separately (a) effect of horizontal permeability through K^* (b) effect of both horizontal and vertical permeability via Da. Since from the definition of Da, when other parameters are kept at constant values, variation of Da indicates the variation of vertical permeability only. The permeability measures the flow strength of the medium and it also acts as a conductivity of the fluid flow. In general high permeability produces the strong flow, whereas, low permeability produces the weak flow. The influence of (K^*) on heat and mass transfer rates is depicted in Figs. 2(a)-(b) at $Da=10^{-4}$, $Ra=2\times10^5$ and $\phi=45^\circ$. From the above figures, it is clear that both bottom as well as side, Nusselt and Sherwood numbers decrease as increasing K^*. Increasing the value of K^*, keeping other parameters constant, implies a decrease of horizontal permeability, consequently reduction of convection in the cavity. Therefore, the average heat and mass transfer rates decrease with increasing K^*. It is natural that reduction of flow by reducing the media permeability causes less over all heat and mass transfer rates.

In order to understand the physics behind this, the contour plots of stream function are plotted in Figs. 3(a)-(f) for different values of K^* at $Da=10^{-4}$, $Ra=2\times10^5$ and $\phi=45^\circ$. It can be observed that the flow in the square cavity governed by two type of convective cells rotating (i) clockwise, (ii) anticlockwise. In anisotropic case one of the cell is dom-

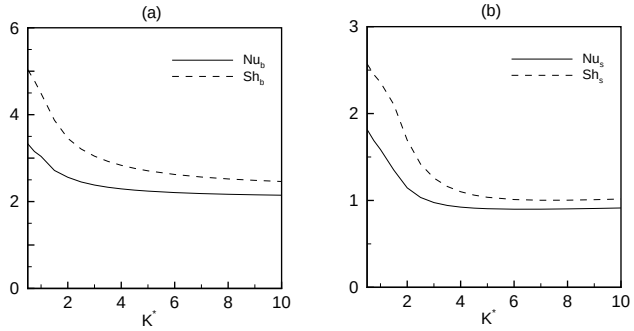

Figure 2: Dependence of the (a) average bottom Nusselt and Sherwood numbers (b) side Nusselt and Sherwood number on permeability ratio (K^*) at $Ra=2\times10^5$, $Da=10^{-4}$ and $\phi=45^\circ$.

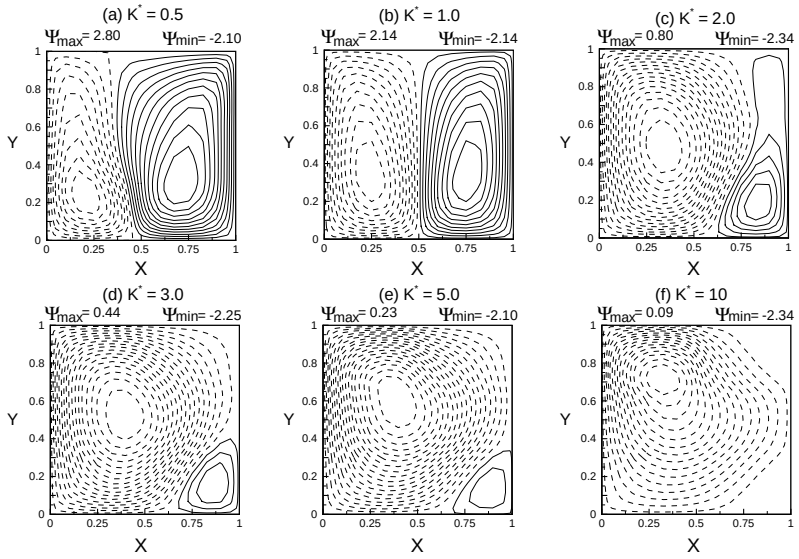

Figure 3: Effect of permeability ratio (K^*) on streamlines at $Da=10^{-4}$, $Ra=2\times10^5$ and $\phi=45^\circ$.

inated on the other one with respect to the value of media permeability and orientation angle. In the streamlines solid lines and dashed lines are associated with a clockwise and anti-clockwise rotation, respectively. When $K^*=1.0$, i.e., isotropic porous media both the cells become mirror image to each other. Further, it is also observed that the maximum magnitude of primary cells (anti-clockwise rotating streamlines) are increased on increasing K^* and secondary cells (clockwise rotating streamlines) are going die out i.e., stream function becomes a unicellular. As a result, the conduction zone near the left side wall is dominated, consequently, both average heat and mass transfer rates decrease on increasing K^*. The change of temperature and concentration profiles as a function of K^* is also observed meticulously from Figs. 4(a)-(f) and Figs. 5(a)-(f) respectively.

The influence of both horizontal and vertical permeability via Da on both heat and

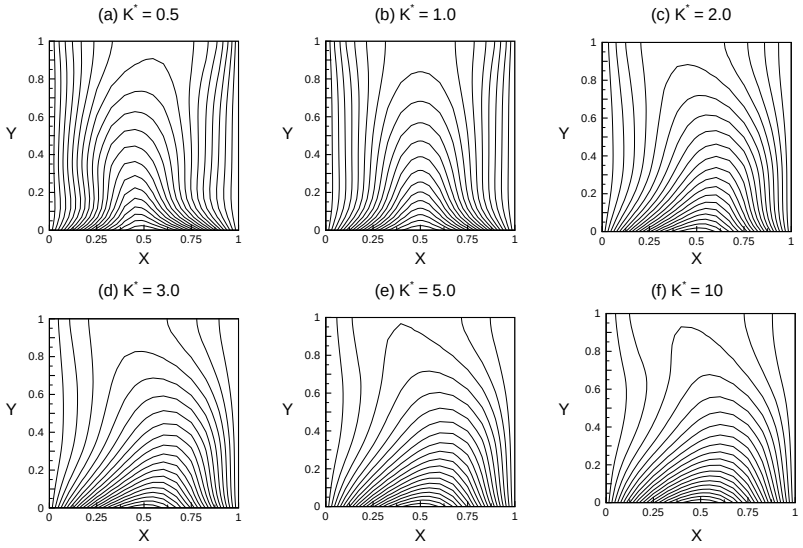

Figure 4: Effect of permeability ratio (K^*) on temperature profile at $Da=10^{-4}$, $Ra=2\times10^5$ and $\phi=45^\circ$.

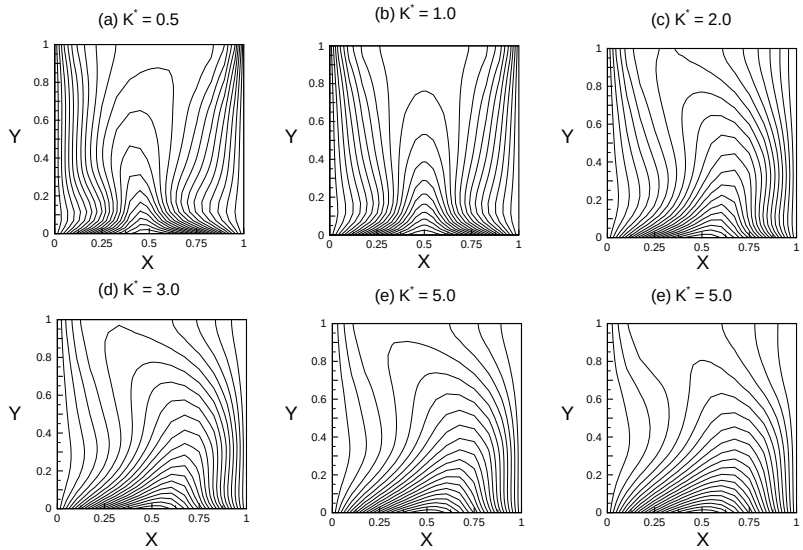

Figure 5: Effect of permeability ratio (K^*) on concentration profile at $Da=10^{-4}$, $Ra=2\times10^5$ and $\phi=45^\circ$.

mass transfers in terms of Nusselt and Sherwood numbers, a comparative study is made below. The effects of Da on both bottom as well as side heat and mass transfer rates for three values 0.5, 1.0 and 2.0 of K^* are plotted in Figs. 6(a)-(c) at $\phi=45^\circ$, $Ra=2\times10^5$. It is observed from above figures, both heat and mass transfer rates on bottom as well as side increase on the enhancement of Da for all values of K^*. which is based on the fact that enhancing Da implies increases of permeability along X as well as Y direction, consequently flow strength increases in the square cavity. Therefore, overall bottom as

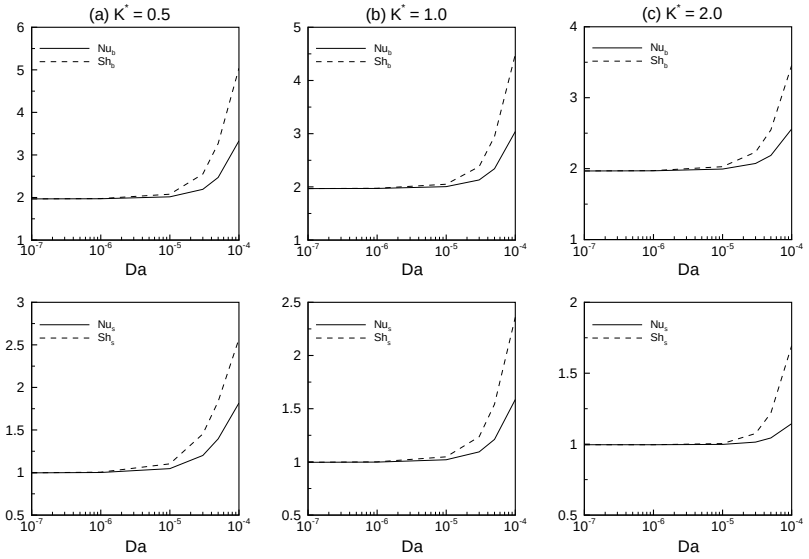

Figure 6: Dependence of the average bottom as well as side Nusselt and Sherwood numbers on Darcy number (Da): (a) $K^*=0.5$, (b) $K^*=1.0$ and (c) $K^*=2.0$ at $Ra=2\times10^5$ and $\phi=45^\circ$.

well as side, heat and mass transfer rates increase on enhancing Da. It can be seen from the Figs. 6(a)-(c) that, for irrespective value of K^*, the heat and mass transfer rates are negligible for $10^{-7}\leq Da\geq 10^{-5}$. However, a significant impact appears on Nusselt and Sherwood numbers when Da lies between 10^{-5} to 10^{-4}.

Furthermore, it can be also found from above figures that, in the range $[10^{-5},10^{-4}]$ of Da, both bottom as well as side mass transfer rate are more than the heat transfer rate. It is due to the choice of physical parameters buoyancy ratio N equal to 2.0. Since the buoyancy ratio (N) is the ratio of species and thermal buoyancy. From the definition of buoyancy ratio, $N=2.0$ means the species buoyancy is twice the thermal buoyancy, consequently, the mass transfer rate is more than the heat transfer rate.

Apart from this, the pattern variation of stream function, temperature and concentration as a function of Da for three different values of K^* (0.5, 1.0 and 2.0) are plotted in Fig. 7, Fig. 8 and Fig. 9 respectively. Fig. 7 shows that, the maximum magnitude of the primary cell is increases on increasing the value of Da for all values of K^*. It is also based on the fact that increases of media permeability along X as well as Y direction, which implies that the flow strength increases in the cavity. Therefore, the above results are expected

3.2 Effect of orientation angle

The effects of anisotropy orientation angle ϕ on the both bottom as well as side Nusselt and Sherwood numbers are depicted in Figs. 10(a)-(b) for $K^*=0.5$ and 2.0 at $Da=10^{-4}$. In case of isotropic porous media i.e., $K^*=1$ both Nusselt and Sherwood numbers are

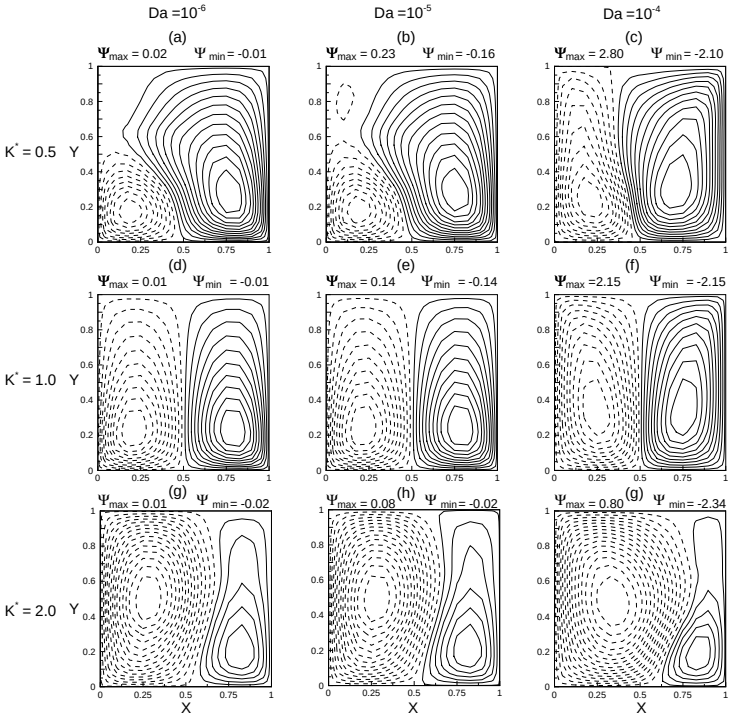

Figure 7: Effect of Darcy Number (Da) on streamlines for different permeability ratio (K^*) at $Ra=2\times10^5$ and $\phi=45^\circ$.

independent of ϕ. From the definition of $\overline{\overline{K}}$, it is clear that the permeability tensor is periodic function of ϕ with period π, so heat and mass transfer rates will also be a periodic functions of same period. As a consequence of it, effect of orientation angle (ϕ) on heat and mass transfer rates is studied in the domain $[0^\circ,180^\circ]$. As can be seen from the Figs. 10(a)-(b) that, first for $K^*=0.5$ and 2.0 both Nu_b and Sh_b attain their maximum values at $\phi=45^\circ$, whereas Sh_s is maximum at $\phi=135^\circ$. Second, Nu_s is attains its maximum (minimum) value at ϕ equal to 45° (135°) for $K^*=0.5$, whereas the same is reverse for K^* = 2 and third, bottom as well as side heat and mass transfer rates are symmetric about the line $\phi=45^\circ$ and $\phi=135^\circ$ in the domain $[0^\circ,90^\circ]$ and $[90^\circ,180^\circ]$, respectively.

To shed some light on this mechanism, stream function contours are plotted for eight values of ϕ (0°, 15°, 30°, 45°, 90°,105°, 120°, 135°) for $K^*=0.5$, and $K^*=5$ are plotted in Fig. 11 and Fig. 12 respectively. For K^* = 0.5 the maximum magnitude of primary cells (anticlockwise rotating streamlines) are increases in the range $[0^\circ,45^\circ]$ (see Fig. 11). Similar trend can also be seen as ϕ varies from 90° to 135° (although the primary cells are clockwise rotating streamlines). In the present study the strength of the primary cells are maximum at ϕ equal to 45° and 135°. As a consequence of it, the maximum bottom heat transfer rate at these values of ϕ is expected. At the same time, a closed look on the stream lines variation as a function of ϕ in the range of $[0^\circ,45^\circ]$ as well as $[90^\circ,135^\circ]$

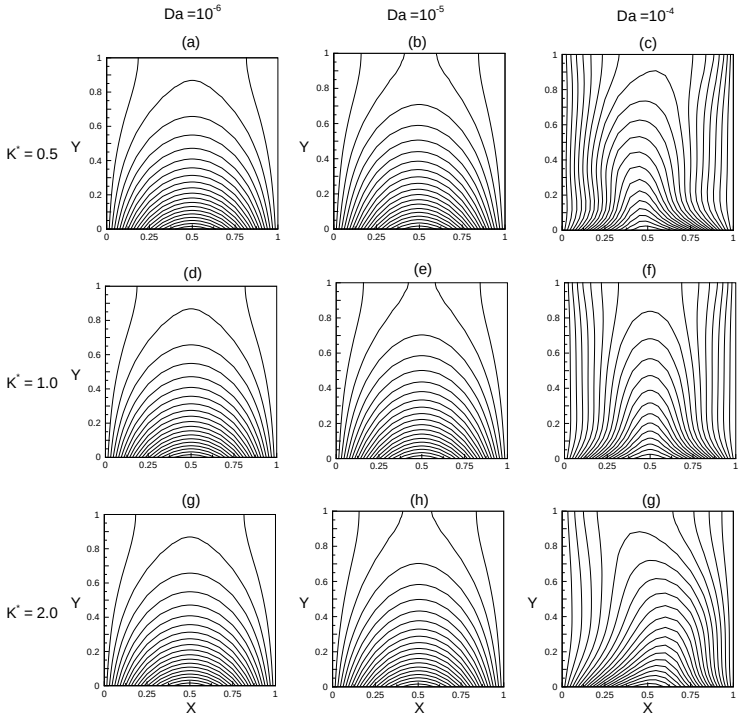

Figure 8: Effect of Darcy Number (Da) on temperature profile for different permeability ratio (K^*) at $Ra=2\times10^5$ and $\phi=45^\circ$.

indicate that as ϕ moves from 0° to 45° the convection region from the left side of the cavity increases. Whereas, the same decreases as ϕ varies from $[90^\circ,135^\circ]$ and it becomes minimum at $\phi=135^\circ$. As a consequence of it Nu_s is minimum for this value of ϕ. The similar change is reverse for $K^*=2.0$. This can be observed from Fig. 12. In this figure we observed that, the convection region from the left side of the cavity increases and it is minimum at $\phi=45^\circ$. As a result, Nu_s attains minimum value at $\phi=45^\circ$. Furthermore, it is to be noted that, overall media permeability, $(K_{xx}=K_{x^*}[a+c])$ along the vertical direction is decreasing as increasing from 0° to 45° for $K^*=2$, the same is changed in reverse way for $K^*=0.5$. This implies, on decreasing media permeability along the main flow direction, it is not necessary that the bottom heat and mass transfer rates will be reduced always.

3.3 Effect of Rayleigh numbers

The impact of Rayleigh number (Ra) on heat as well as mass transfer rates in an anisotropic porous medium is depicted in Figs. 13(a)-(d) for three values 0.5, 1.0 and 5 of K^* at $\phi=45^\circ$, and $Da=10^{-4}$. From the above figure, for isotropic as well as anisotropic media, effect of Rayleigh number on bottom as well as side average heat and mass transfer rates (Nusselt and Sherwood numbers) become significance beyond $Ra=10^4$. It is also

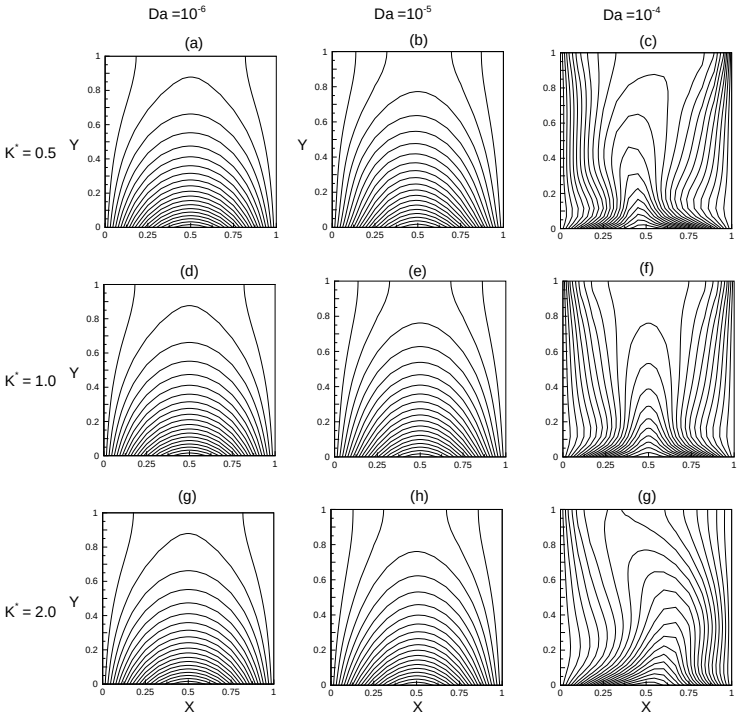

Figure 9: Effect of Darcy Number (Da) on concentration profile for different permeability ratio (K^*) at $Ra=2\times10^5$ and $\phi=45^\circ$.

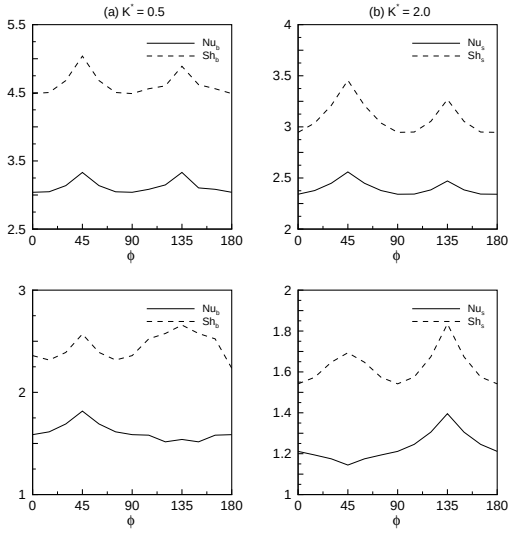

Figure 10: Variation of average Nusselt numbers (Nu_b as well as Nu_s) and Sherwood numbers (Sh_b as well as Sh_s) as a function of orientation angle (ϕ) for different values of K^*; (a) $K^*=0.5$ and (b) $K^*=2$, when $Da=10^{-4}$ and $Ra=2\times10^5$.

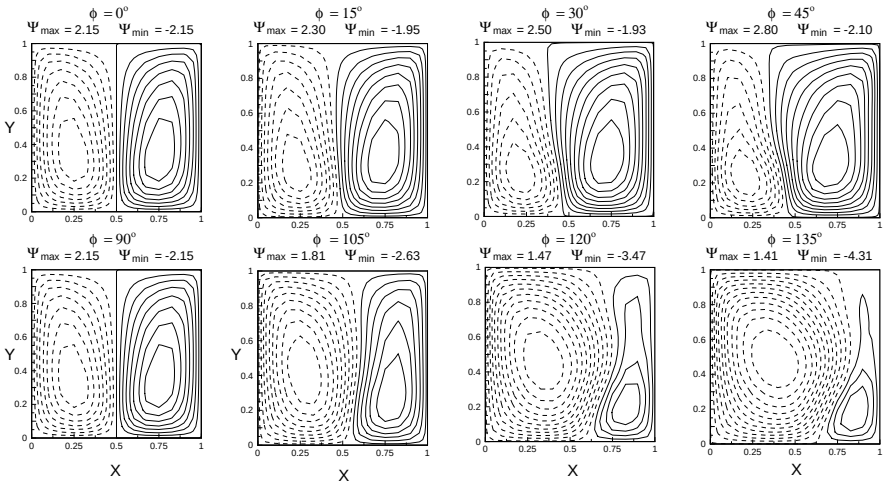

Figure 11: Effect of orientation angle on streamlines for $K^*=0.5$, at $Ra=2\times10^5$ and $Da=10^{-4}$.

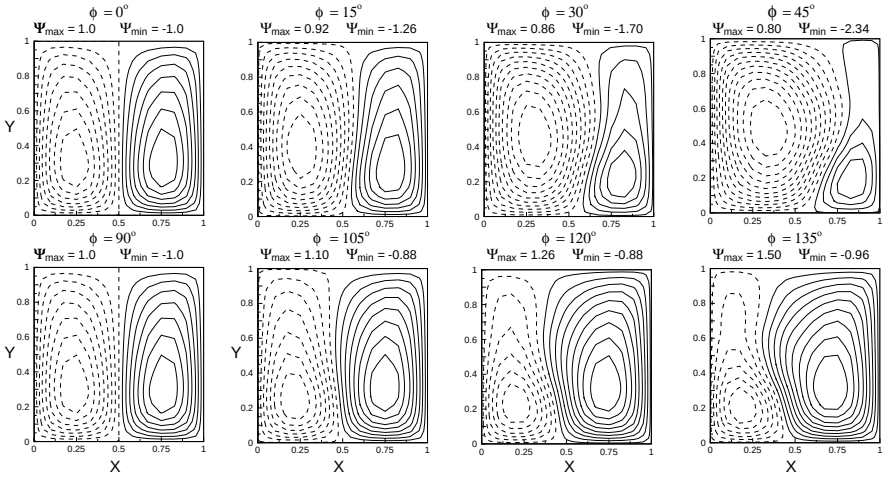

Figure 12: Effect of orientation angle on streamlines for $K^*=2.0$, at $Ra=2\times10^5$ and $Da=10^{-4}$.

observed that, both heat and mass transfer rates increase on increasing Rayleigh number (Ra) for all the values of K^*. From the definition of Ra, when other parameters are fixed, increasing of Ra implies the enhancement of thermal buoyancy force, which in turn to increases the thermal convection in the cavity. As a result, the average bottom as well as side average heat and mass transfer rates are expected to increase.

4 Conclusions

In the present study, a numerical study of thermo-solutal natural convection in a square cavity filled with anisotropic porous medium is investigated. The flow is induced by a

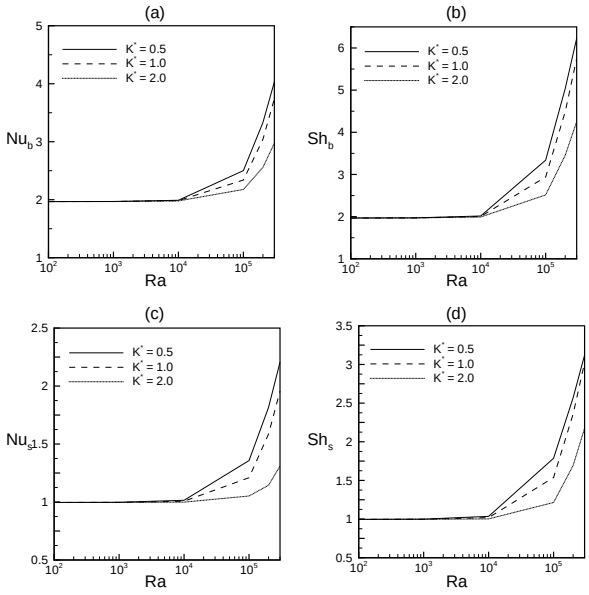

Figure 13: Variation of average Nusselt numbers (Nu_b as well as Nu_s) and Sherwood numbers (Sh_b as well as Sh_s) as a function of Rayleigh number for different values of K^*; when $\phi = 45^\circ$, and $Da = 10^{-4}$.

sinusoidally varying temperature and concentration distribution of the bottom wall, and buoyancy force, when other two vertical walls are mentioned a constant temperature and concentration. The non-Darcy Brinkmann model is adopted to simulate the momentum transfer in the porous medium. Spectral element method is adopted to solve the governing differential equations numerically. The main objective in this study is to investigate the effect of anisotropic parameters: (i) orientation angle of media permeability tensor (ϕ) and (ii) permeability of the media through Darcy number (Da), permeability ratio (K^*) as well as Rayleigh number (Ra) on the flow mechanism and consequently on the average bottom as well as side heat and mass transfer rates. The following conclusions can be drawn from this study.

1. Both bottom as well as side, Nusselt and Sherwood numbers decrease on increasing K^*. Increasing the value of K^*, keeping other parameters constant, implies a decrease of horizontal permeability, consequently reduction of convection in the cavity.
2. Two types of convective cells, (i) rotating clockwise way (ii) rotating anticlockwise way, are observed in the entire flow mechanism and depending on the media permeability one cell dominates on the other.
3. For all value of K^* (considered this study), the heat and mass transfer rates are negligible for $10^{-7} \leq Da \geq 10^{-5}$, $Ra = 2 \times 10^5$ and $\phi = 45^\circ$. However a significant impact on Nusselt and Sherwood numbers when Da lies between 10^{-5} to 10^{-4} is observed.

4. Average bottom as well as side heat and mass transfer rates are symmetric about the line $\phi=45^\circ$ and $\phi=135^\circ$ in the domain $[0^\circ,90^\circ]$ and $[90^\circ,180^\circ]$ respectively. Furthermore, the maximum bottom heat and mass transfer rates (Nu_b, Su_b) is attained at $\phi=45^\circ$, when $K^*=0.5$ and 2.0.
5. The both heat and mass transfer rates increase on increasing Rayleigh number (Ra) for all the values of K^*.
6. The present investigation shows that, the effect of the anisotropic permeability and permeability orientation angle on the flow is complex.

Acknowledgments

One of the authors, Ashok Kumar, is grateful to University Grants commission India for providing financial assistance under the under BSR startup grant (No. F.30-57/2014(BSR)) duing the preparation of this manuscript.

References

[1] R. W. SCHMIDT, *Double diffusion in oceanography,* Ann. Rev. Fluid Mech., 26 (1994), pp. 255–285.
[2] D. A. NIELD AND A. BEJAN, Convection in Porous Media, Springer, New York, 2006.
[3] Y. KAMOTANI, W. WANG, S. OSTRACH AND H. D. JIANG, *Experimental study of natural convection in shallow enclosures with horizontal temperature and concentration gradients,* Int. J. Heat Mass Transf., 28 (1985), pp. 165–173.
[4] J. LEE, M. T. HYUN AND K. W. KIM, *Natural convection in confined fluids with combined horizontal temperature and concentration gradients,* Int. J. Heat Mass Transf., 31 (1969), pp. 1969–1973.
[5] C. BEGHEIN, F. HAGHIGHAT AND F. ALLARAD, *Numerical study of double diffusive natural convection in square cavity,* Int. J. Heat Mass Transf., 35 (1992), pp. 833–845.
[6] R. BENNACER AND D. GOBIN, *Cooperating thermosolutal convection in enclosures-I, scale analysis and mass transfer,* Int. J. Heat Mass Transf., 39 (1996), pp. 2671–2681.
[7] R. BENNACER AND D. GOBIN, *Cooperating thermosolutal convection in enclosures-II, heat transfer and flow structure,* Int. J. Heat Mass Transf., 39 (1996), pp. 2683–2697.
[8] K. GHORAYEB AND A. MOJTABI, *Double diffusive convection in vertical rectangular cavity,* Phys. Fluid, 9 (1997), pp. 2339–2348.
[9] A. SEZAI AND A. A. MOHAMAD, *Double diffusive convection in a cubic enclosure with opposing temperature and concentration gradients,* Phys. Fluid, 12 (2000), pp. 2210–2223.
[10] O. V. TREVISAN AND A. BEJAN, *Mass and heat transfer by natural convection in a vertical slot filled with porous medium,* Int. J. Heat Mass Transf., 29 (1986), pp. 403–415.
[11] K. N. MEHTA AND K. NANDKISHOR, *Natural convection with combine heat and mass transfer buoyancy effects in non homogeneous porous medium,* Int. J. Heat Mass Transf., 30 (1987), pp. 2651–2656.
[12] M. MAMOU, P. VASSEUR AND E. BILGEN, *Multiple solutions for double diffusive convection in vertical porous enclosure,* Int. J. Heat Mass Transf., 38 (1995), pp. 1787–1798.

[13] M. MAMOU, P. VASSEUR AND E. BILGEN, *Analytical and numerical study of double diffusive convection in vertical enclosure,* Int. J. Heat Mass Transf., 32 (1996), pp. 115–125.
[14] O. V. TREVISAN AND A. BEJAN, *Natural convection with combine heat and mass transfer buoyancy effects in porous medium,* Int. J. Heat Mass Transf., 28 (1985), pp. 1997–1611.
[15] B. GOYEAU, J. P. SONGBE AND D. GOBIN, *Numerical study of double-diffusive natural convection in a porous cavity using the Darcy-Brinkman formulation,* Int. J. Heat Mass Transf., 39 (1996), pp. 1363–1378.
[16] J. KRAMER, R. JECL AND L. SKERGET, *Boundary domain integral method for the study of double-diffusive natural convection in a porous media,* Eng. Ana. Bou. Element, 31 (2007), pp. 897–905.
[17] F. ALAVYOON, *On natural convection in vertical porous enclosures due to prescribed fluxes of heat and mass at the vertical boundaries,* Int. J. Heat Mass Transf., 36 (1993), pp. 2479–2498.
[18] F. ALAVYOON, Y. MASUDA AND S. KIMURA, *On natural convection in vertical porous enclosure due to opposing fluxes of heat and mass prescribed at the vertical walls,* Int. J. Heat Mass Transf., 37 (1994), pp. 195–206.
[19] P. NITHIARASU, K. N. SEETHARAMU AND T. SUNDARARAJAN, *Double-diffusive natural convection in an enclosure filled with fluid saturated porous medium: A generalized non-Darcy approach,* Numer. Heat Transf. Part A, 30 (1996), pp. 413–426.
[20] P. BERA, V. ESWARAN AND P. SINGH, *Numerical study of heat and mass transfer in an anisotropic porous enclosure due to constant heating and cooling,* Numer. Heat Transf. Part A, 34 (1998), pp. 887–905.
[21] P. BERA, V.ESWARAN AND P. SINGH, *Double-diffusive convection in slender anisotropic porous enclosure*, J. Porous Media, 3 (2000), pp. 11–29.
[22] P. BERA AND A. KHALILI, *Double-diffusive natural convection in an anisotropic porous cavity with opposing buoyancy forces: Multi-solutions and oscillations,* Int. J. Heat Mass Transf., 45 (2002), pp. 3205–3222.
[23] R. BENNACER, A. TOBBAL, H. BEJI AND P. VASSEUR, *Double diffusive convection in a vertical enclosure filled with anisotropic porous media*, Int. J. Thermal Sci., 40 (2001), pp. 30–41.
[24] A. KUMAR AND P. BERA, *Natural convection in an anisotropic porous enclosure due to non-uniform heating from the bottom wall,* ASME J. Heat Transf., 131 (2009), 07260-1-13.
[25] M. S. MOJTABA AND S. M. REZA, *Invistigation of natural convection in a vertical cavity filled with a anisotropic porous media,* Iran J. Chemistry Chem. Eng., 27 (2008), pp. 39–45.
[26] S. SAFI AND S. BENISSAAD, *Heat and mass transfer in anisotropic porous media,* Adv. Theoretical Appl. Mech., 5 (2012), pp. 11–22.
[27] A. T. PATERA, *A Spectral element method for fluid dynamics: Laminar flow in a channel expansion,* J. Comput. Phys., 54 (1984), pp. 468–488.
[28] C. CANUTO, M. Y. HUSSAINE, A. QUARTERONI AND T. A. ZANG, Spectral Method in Fluid Dynamics, Springer, New York, Berlin Heidelberg, 1986.
[29] G. NEALE, *Degrees of anisotropy for fluid flow and diffusion (Electrical Conduction) through anisotropic porous media,* AIChE. J., 23 (1977), pp. 56–62.
[30] P. A. TYVAND, *Thermohaline instability in anisotropic porous media,* Water Res. Resources, 16 (1980), pp. 325–330.